Ferroelectrics, 475: 135–147, 2015

ISSN: 0015-0193 print / 1563-5112 online
DOI: 10.1080/00150193.2015.995580

Taylor & Francis
Taylor & Francis Group

Modified Hydroxyapatite Structure and Properties: Modeling and Synchrotron Data Analysis of Modified Hydroxyapatite Structure

A. V. BYSTROVA,[1,2] YU. D. DEKHTYAR,[2] A. I. POPOV,[3] J. COUTINHO,[4] AND V. S. BYSTROV[1,5,*]

[1]Institute of Mathematical Problems of Biology RAS, 142290 Pushchino, Russia
[2]Biomedical Engineering and Nanotechnology Institute, Riga Technical University, Riga, Latvia
[3]Institute M. von Laue - P. Langevin, Grenoble, France
[4]Physics Department, University of Aveiro, Aveiro, Portugal
[5]Department of Material Engineering and Ceramics & CICECO, University of Aveiro, Aveiro, Portugal

First principle modeling and calculations of hydroxyapatite both native and surface modified and having various defects (OH vacancies, H inter-nodes) were performed. Local Density Approximation method used with calculations of Density of States allows us to analyze the experimental obtained work function data. Molecular modeling was confirmed by photo-electron measurements up to 6.5 eV and photoluminescence experimental data from synchrotron DESY up to 30 eV. Brief analysis of the influence of heating, microwave radiation, hydrogenation, and synchrotron radiation on hydroxyapatite surface is presented in this work. New data on the structure of modified hydroxyapatite are obtained.

Keywords Hydroxyapatite; modeling; DOS; work function; photo-electron; photoluminescence; defects; vacancies; inter-nodes

1. Introduction

Hydroxyapatite (HAP) is one of the most demanded materials in implantology of bones and teeth [1–5]. The main application area is HAP coating on bones and dental implants in order to modify their surface properties for the best osseointegration [1, 2]. Biological HAP differs from the mineral one: it consists of many deviations, such as non-stoichiometry content, replacements, vacancies, and other defects. As it was established in several experimental works and in the project PERCERAMICS [5], interaction between HAP biomaterials and living cells (particularly, such as osteoblasts) is improved, if the HAP surface is charged or polarized [3–5]. This result is confirmed by studies of charged HAP performed in Refs. [6, 7]. Additionally, it was found that HAP surface geometry was influenced by interaction with living cells [4, 7]. The influence of environment (pH

Received July 15, 2014; in final form September 30, 2014.
*Corresponding author. E-mail: bystrov@ua.pt, vsbys@mail.ru
Color versions of one or more of the figures in the article can be found online at www.tandfonline.com/gfer.

index, citrate content, etc.) was revealed too [3, 8]. Besides, the HAP nanoparticles size and shape were demonstrated to vary in interactions with living cells [3, 4, 7, 8]. However, many details of the mechanism are still unclear. The examples are influences of various defects (vacancies, inter-nodes, etc.), formation of the surface charges and the interaction between electric charges, surface potential, and living cells (osteoblasts and other osteo-cells leading to bone tissues formation) on the HAP surface. Some attempts and results obtained with the use of the first principle Local Density Approximation (LDA) and Density of States (DOS) calculations have been presented recently in Ref. [9]. Several papers reported HAP structural peculiarities and physical properties obtained by various theoretical computational approaches [10-–14] and experimental methods [15]. Some further studies are developed in Refs. [16, 17].

We consider here some calculations of surface modified HAP (which calls for further investigation of the interaction with living cells based on this approach). The aim of this work was to look at deeper levels of electron excitation of HAP for more clear understanding of its deepest structure and influence of such defects as vacancy and inter-node, especially hydrogen atoms (protons) and hydroxyl groups (OH). The photoelectron excitation technique allows us to see the result of usual excitation only at the levels up to 6 eV. Synchrotron technique gives us an opportunity to study the electron excitations up to 35 eV. As HAP is widely used, it is necessary to study its properties under the influence of various factors to predict the behavior inside living structures.

2. Main Computational Methods and Models

In this work, we make calculations using the density functional theory (DFT) in local density approximation (LDA) [9, 14] in AIMPRO code [17, 18]. This method also involves a pseudo-potentials approach for calculations of each atomic potential and wave function. For this purpose, we use here the standard valence configurations for hydrogen (1s1), phosphorus (3s2_3p3), and oxygen (2s2_2p4). But for calcium we use two different valence configurations: 1) “Ca2” with 2 valence electrons (4s2) shell, and most accurate 2) “Ca10” with 10 valence electrons (3s2_3p6_4s2) shell. The cutoff of the kinetic energy for bulk calculations was at the level of 300 a.u. The best Monkhorst–Pack k-point meshes for the Brillouin Zone (BZ) integration of hexagonal and monoclinic primitive cells were found to be $2 \times 2 \times 4$. The initial lattice unit cell for hexagonal HAP structure consists of 44 atoms, while for monoclinic HAP nanostructures it consists of 88 atoms, because the lattice unit cell is doubled in the latter monoclinic case along b axis. For super-cell model calculations we use 88 and 176 atoms, respectively. In all the calculations – except the elastic constant calculations – we take into account the full cell relaxation, including changing the volume and adjusting the atomic positions and cell shape. For molecular modeling we use HyperChem [19].

First, we constructed the lattice unit cell models for both hexagonal and monoclinic HAP phases. We used modeled and computed data from HAP nanoparticle models [3] as first approximations for the lattice unit cell. The experimental data were taken from Refs. [10, 11], the data of calculations were from Refs. [11–13]. Several new data computed and used here were published recently in Refs. [14, 16, 17].

3. Experimental Methods and Materials

Initially, 12 samples of HAP (preliminary fabricated before this study as described in Ref. [5]) were selected randomly. The following scheme of investigation was applied to them.

First, the photo-emission spectrum (i.e., intensity of photoelectron emission (PE) current versus photo-excitation energy) of each sample was measured using a setup, assembled from MSD-2 monochromator, ultraviolet light Xe-Hg source Hamamatsu, and a vacuum chamber from KURT J. LESKER, Geigerzähler Dosimeter Strahlenmessgerät Robotron 20046 (dosimeter Geiger Robotron 20046). Subsequently, different processing treatment schemes were applied to the different samples as shown in the scheme (Fig. 1). Two samples were control ones without any treatment. The values of the electron work function φ were estimated with an error of less than ±0.04 eV. It is comparable with the error in calculation of the density of electronic states (DOS) data in this work ~ ±0.05 eV. Selected HAP samples were heated for 30 minutes at the temperature of 542–546^{o}C under a pressure of (7.5-–8.7)*10^{-6} Pa, which was obtained at a heating rate of 15 degrees per minute. Hydrogenation was carried out in special chamber for 6 hours at pressure of 60 ± 2 atmospheres, T = 23°C. Microwave radiation was applied with power of 800 W for 6.5 min. Ionizing radiation was applied at a dose of 1MGray. After that a control measurement of the photo-emission spectrum was made again.

Then, all the samples were sent to a group of Dr. A. Popov for synchrotron irradiation studies on DESY (Deutsches Elektronen-Synchrotron, Hamburg). Some samples were randomly selected there and investigated using varying wavelengths of excitation. Photoluminescence (PL) emission was measured. First, we tried to find the most important PL emission spectral line after initial excitation with 180 nm wavelength, corresponding to energy 6.89 eV, which is much greater than all known data of energy of HAP forbidden band gap width $Eg = Ec - Ev$, where Ec is a bottom of conductance band and Ev is a top of valence band. Second, after determination the PL wavelength corresponding to the main PL intensity peak, we conduct registration of PL emission spectra at this spectral line with the excitation in full energy range λ = 333–80 nm (energy 3.72–15.5 eV). This is standard procedure used for the PL measurements with synchrotron irradiation [20]. After bringing samples back, their photo-emission spectrum was measured again by the above described technique.

4. Experimental Data

After performing the experimental work, we have processed all the obtained data to find the most essential and important results. Having reviewed the entire data set after treatments, we have found that the maximum of radiation intensity as a function of

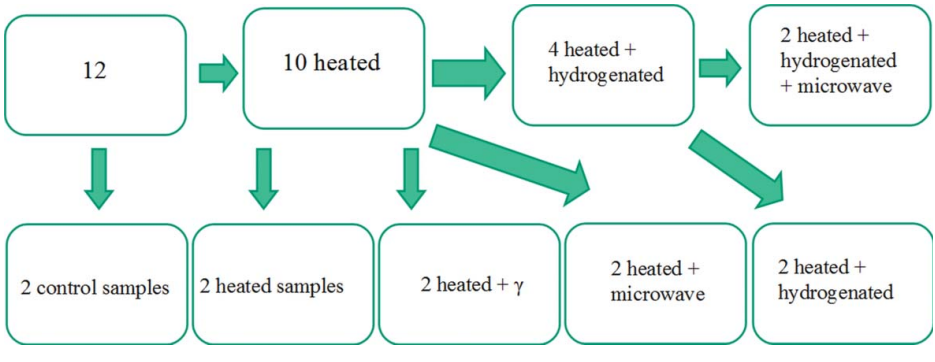

Figure 1. Scheme of HAP samples processing.

wavelength is observed in the range of 4.6–5.4 eV, corresponding to work function values of usual bulk HAP crystal. We evaluated also the effects of various treatments factors, described above. For example, variations of common effects of hydrogenation, microwave radiation, and heating processes are presented in Fig. 2.

The corresponding variations of electron work function *Aex* are presented in Fig. 3. In general, the variations of *Aex* are around values (Fig. 3a): 5.25 eV for case 1, 5.04 eV for case 2, and 5.24 eV for case 3. However, after some treatment (e.g., heating/microwave) *Aex* was ~3.75 eV (Fig. 3b) for case 2. But the main result was obtained from the synchrotron spectrum after heating and microwave irradiation, and sometimes after hydrogenation of HAP (Figs. 4, 5).

The data obtained on the initial emission of PL spectrum (Fig. 4) suggest that for all kinds of the sample treatments there is only one main PL energy level with energy $Ei = \sim 2.95$ eV (or with wavelength ~420 nm). But the main rises of intensity for this energy level are observed after heating (T), heating with Xray, heating with microwave (MW) irradiation and with hydrogen (H_2) (curves 7, 8, 10, 6, 3 in Fig. 4). This fact means that after corresponding treatments we obtain an increase of some defects concentration in the HAP samples, which have recombinant energy level in the forbidden band with value of *Ei* ~2.95 eV ~3 eV (or 420 nm line) from

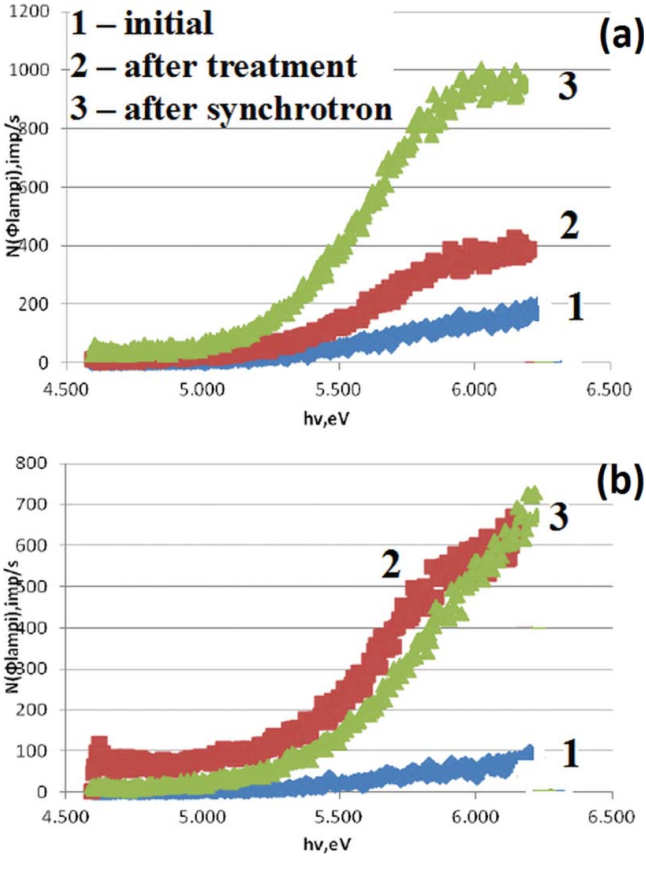

Figure 2. Intensity of the PE current after the influence of heating (a) and microwave radiation (b).

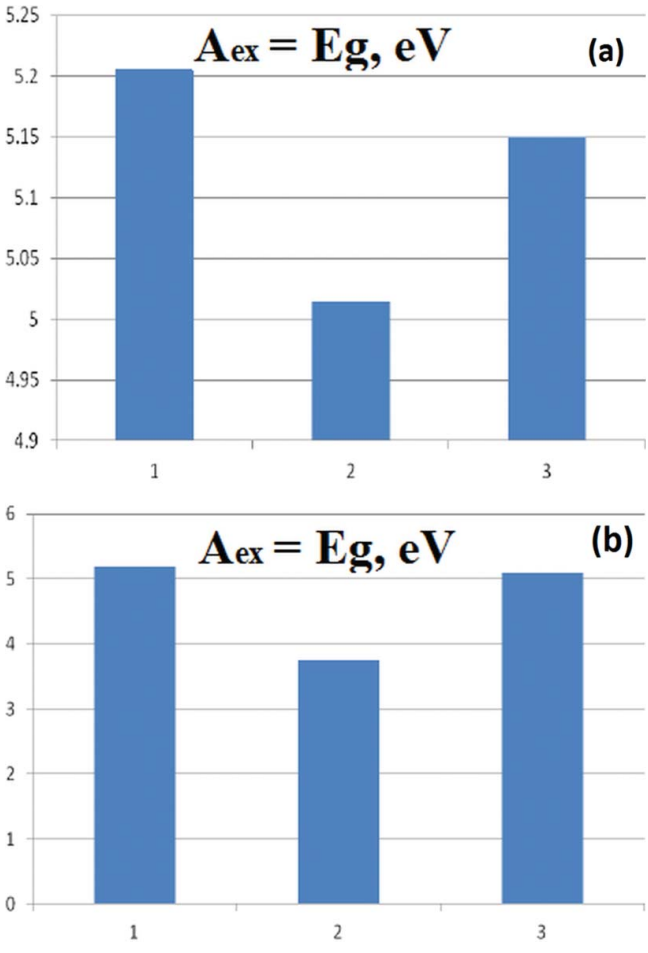

Figure 3. Values of the electron work function (corresponding to data in Fig. 2a,b): 1 – the original electron work function A_{ex} before any influences, 2 – after the applied effects, such as microwave radiation, hydrogenation, and heating, 3 – after the synchrotron radiation.

the bottom of the conductance band. We suppose that the origin of this defect might be both OH vacancy and H internodes (see discussion below). Corresponding increase of intensity after the treatments is 27–45%.

After that we measured the excitation PL spectrum of this 420 nm line in the whole energy range from 4 up to 16 eV. Figure 5a shows the total spectrum obtained, while in Fig. 5b details of high energy spectrum from 8 up to 16 eV are presented.

It is well known that HAP formula is $Ca_5(PO_4)_3(OH)$. The preliminary analysis leads to the conclusion that the observed high energy peaks at ~9–10.5, 11–12, 13–14 eV most likely match the first ionization potential (IP) of the phosphorus atom P (which is close to the isolated atom with the value ~10.5 eV), the second IP of the calcium atom Ca (which is ~11.87 eV for the isolated atom, while the first IP ~6 eV is usually close to the forbidden band of HAP crystal) and the first IP of the oxygen atom (which is ~13.6 eV for isolated atom). The latter value also corresponds to the IP ~13.6 eV of the isolated hydrogen atom.

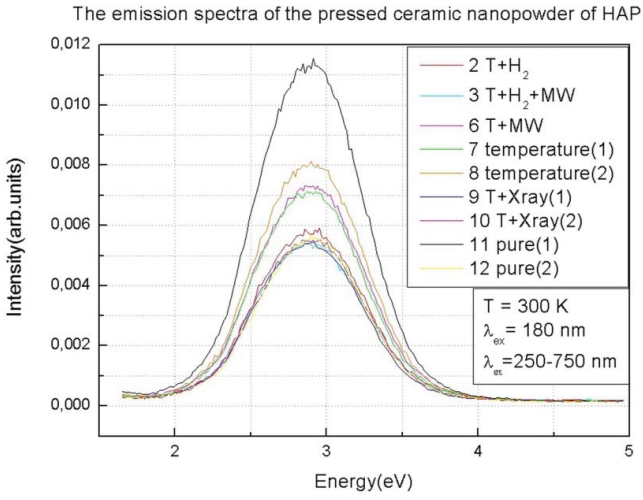

Figure 4. Data of the synchrotron emission PL spectrum. Intensity maximum for all peaks is approximately at the E $\sim$ 2.95 eV (with corresponding PL wavelength $\lambda = 420$ nm). The average half-width of the peaks is $\sim$1 eV in range from $\sim$2.4 eV up to $\sim$3.4 eV.

From the calculations of the DOS for HAP crystal it is known [9, 13, 16] that these energy peaks for the first P 3s and P 3p orbitals, Ca 3D + 4S orbitals, O 2P orbitals, and H 1S orbitals have approximately the same energies as reckoned from the bottom of the conductive band. Notice that the forbidden gap is equal to $Eg \sim 4.6 - 5.4$ eV [17]. Thus, the obtained energy differences are of the same order of magnitude for the excitation of electrons from these orbitals of HAP. This conclusion requires detailed examination and this issue is in process. Below we consider some of models, calculations, and interpretations of the data obtained.

5. Results and Discussion

First, one of the most interesting computational results is that for the monoclinic unit cell the energy $= -934.20024$ a.u. (having divided this value by two in order to compare primitive unit cells) / $2 = -467.10012$ a.u., which lies below the energy of the hexagonal unit cell equal to $= -467.\ 09923$ a.u. The energy difference is $\Delta E = 0.00089$ a.u. $=$ 0.024218 eV $\sim$ 24.2 meV. This result is comparable with Ref. [12], where the energy difference was found to be $\sim$22 meV, and confirms the data about possible coexistence of monoclinic and hexagonal HAP phase at room temperature. Notice that the thermal energy at room temperature is $\sim$25 meV. For more detail see Refs. [9, 14, 17].

Second, the other important result is that we calculated the DOS distributions for initial optimized HAP lattice and for all atomic positions. We obtained the value of the forbidden gap Eg [9, 14, 17], which is very close to the reported data, though the data vary depending on the approximation used (Eg $\sim$ 4.98 eV for model 10 Ca electrons "Ca10" shell, Eg $\sim$ 4.6 eV for model "Ca2" shell) [9, 14, 17]. The values of Eg obtained in this study are consistent with the calculations by other authors, such as Refs. [10–14].

Calculation of DOS also allows us to study the influence of lattice's charges on the shift and changes of Eg, which are in good agreement with experimental data on living cells attachment to charged HAP surface [3, 6–9].

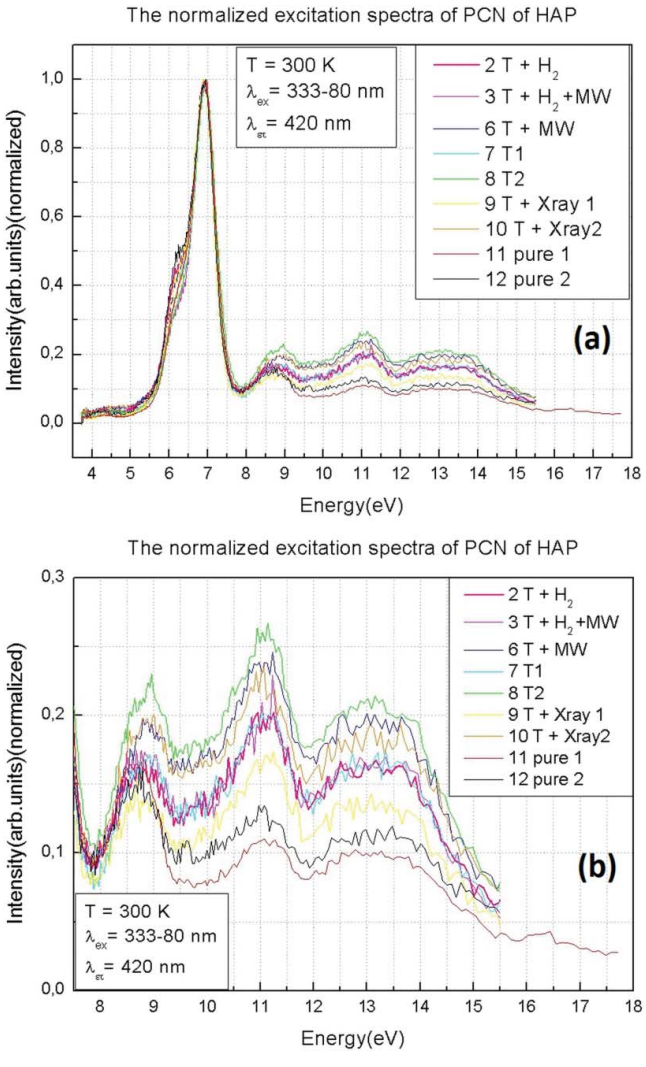

Figure 5. Data of the synchrotron excitation spectrum in the total range of λ ex = 333 – 80 nm (corresponding energy 3.7–15.5 eV) for registration of PL at λ = 420 nm (equivalent to ~2.95 eV): (a) total range, (b) only at the high energy range.

Experimentally, it was possible to create an excess charge in the surface layers of HAP, by placing the sample in a chamber filled with hydrogen at high pressure. This process is called *hydrogenation* [7]. We suppose that during the hydrogenation process the introduced hydrogen atoms could create both interstitial/inter-nodes and vacancies (O or OH types). But, heating and microwave irradiation could also give an opportunity for protons to jump through OH-channels energy barriers inside HAP surface layers [4]. We calculated DOS for initial HAP state and HAP with several defects. For pure HAP structure we obtained only a shift of DOS energy levels with change of the cell unit charge [9]. One of the important features is that one OH vacancy per unit cell leads to a shift of the forbidden gap to higher value Eg ~ 5.49 eV for "Ca2" model [17] (Fig. 6).

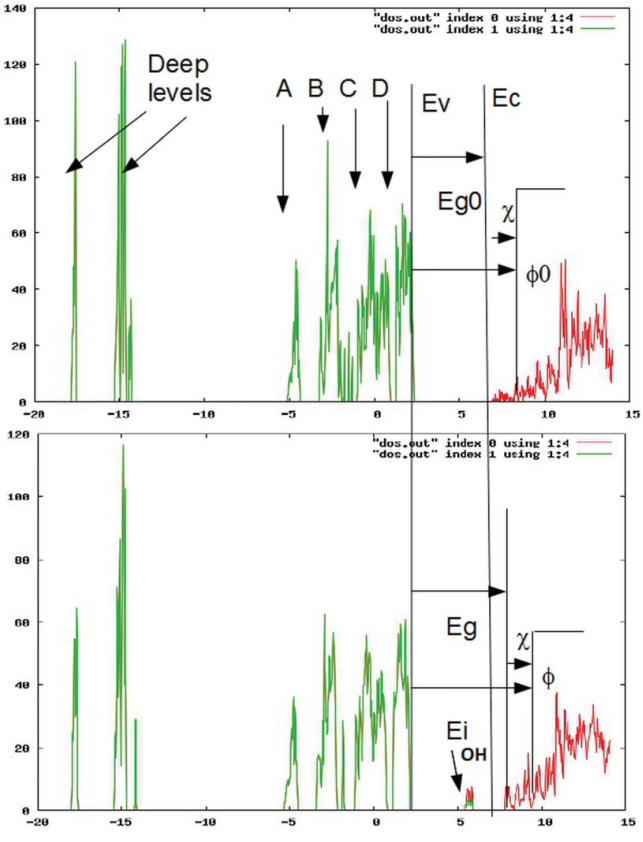

Figure 6. Density of states (DOS) for initial pure HAP hexagonal structure in "Ca2" model (upper image) and DOS for the case with one OH vacancy per unit cell (down image). Green color marked occupied states and red – unoccupied. A, B, C, and D – main peaks in HAP valence band, corresponding to known data [12, 13]; Ev – is valence band top, Ec – is conductive band bottom, Eg = Ec – Ev, φ is the electron work function and χ is the electron affinity, $\varphi = \chi + \text{Eg}$. For OH vacancy arisen additional energy levels (narrow band) are shown as Ei (OH) and it is half-occupied in normal state. The average energy Ei $\sim$ Ev + (3.0 – 3.8) eV $\sim$ Ec – (2.5 – 1.7) eV.

It is interesting that, if one excess hydrogen is introduced into one unit cell (e.g., for hexagonal phase with LDA "Ca2" model), we observe (apart from a small shift of all energy levels) arising of strong additional energy levels inside the forbidden gap Eg. The average energy of these levels are approximately Ei $\sim$ Ev + (1.2 – 1.75) eV from the top of the valence band Ev, or Ei $\sim$ Ec – (3.9 – 3.4) eV from the bottom of the conductive band Ec (Fig. 7) [17].

For a vacancy of one hydrogen atom we obtain an additional energy level, which is very close to the top of the valence band: $\text{Ei} = \text{E}_{\text{H-vac}} = \sim \text{E}_\text{v} + (0.1 - 0.2)$ eV. For OH vacancy we obtained deep energy levels: $\text{Ei} = \text{E}_{\text{OH-vac}} = \text{E}_\text{v} + (3.0 - 3.8)$ eV $\sim$ Ec – (2.5 – 1.7) eV, which are more close to the bottom of the conductive band (Fig. 6) [17]. The latter results are very similar to the data reported in Ref. [13]. It should be noted that the experimentally observed surface level with energy E5 = Ev + 3.3 eV [15] is very close to our values. But the nature of this surface level is not clear in Ref. [15]. Now we can conclude that these several levels or the narrow energy band in the middle of the

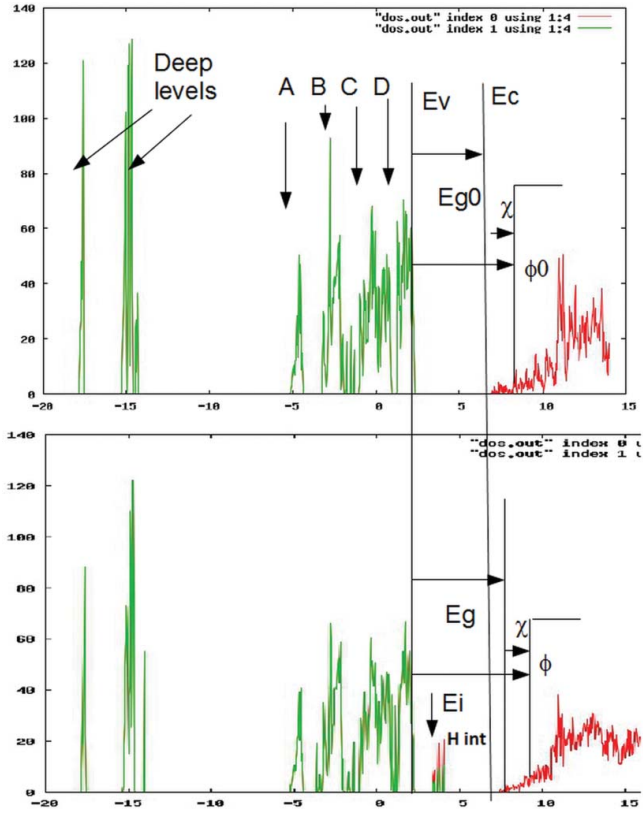

Figure 7. DOS with one additional inserted hydrogen atom H per HAP hexagonal unit cell (down image) in comparison with DOS of the initial pure HAP hexagonal structure. Inserted H is positioning in columnar OH-channel of HAP between two OH groups and its energy level (on DOS scheme) inside forbidden zone is marked as Ei (H int). This H inter-node has three narrow half-occupied states with average energy Ei ~ Ev + (1.2 – 1.75) eV ~Ec – (3.9 – 3.4) eV.

forbidden gap Eg must belong directly to the OH-vacancy, which may exist at higher concentrations in HAP surface layer [16].

It is important that the HAP samples used had *p*-type semiconducting property, confirming that it is recombinant hole levels, which trapped electrons from the conductive band. As a result, we obtain the PL emission, when electrons are trapped by this level. The authors of Ref. [15] supposed that it might be OH vacancies, which could rise after heating. Now we can confirm that it must be OH-vacancy in the HAP surface layer. The PL intensity at the 11 eV increases 3–3.7 times in the case of heating (8 T2) and heating with microwave (6 T + MW), which is close to Ref. [15] in the case of OH annealing at high temperature. Another important model might be concerned with inserted proton into HAP structure through OH-channel. In this case we obtain the overlapped electron orbitals, which could serve as some intermediate state for further electron transitions from the excited state to the trapped one [16].

Calculation of the DOS allows us to determine not only the forbidden energy gap Eg = Ec – Ev, but also the changes of the Eg value and the formation of additional energy levels Ei, which correspond to several modeled defects of HAP unit cell structure. Let us consider

shortly the main schemes of computed DOS structures (Fig. 6, upper image), which present possible connections with photoelectron emission experimental data. The upper DOS image in Fig. 6 presents the DOS structure of the initial pure hexagonal HAP and consists of several peaks (A, B, C, and D) in the valence band and several deep levels, which are in good agreement with the data obtained by other authors [10-14]. In our case we can also mark by "green" color all the states and energy levels, which are occupied by electrons, and by "red" color – unoccupied energy levels and bands (such as, e.g., conductive band). When photoelectric excitation is applied to samples with sufficient energy (e.g., equal and larger than the forbidden band width gap Eg = Ec – Ev), electrons can excite to conduction zone. If then additional energy is applied, equal and larger than the electron affinity χ, then electrons obtain the total energy $\varphi = \chi + \mathrm{Eg}$ and can escape from HAP sample being collected by a detector. This border energy level is electron work function φ, measured by photoelectron emission technique (see, e.g. [16]). For further analysis we introduce here Eg_0 and φ_0 as energy gap and work function for initial pure HAP, while for all the cases with defects influences, etc., the modified new values are Eg and φ. Supposing that electron affinity changes only slightly ($\chi \sim$ const $\sim$ 1 eV [15]), we can compare our calculated data of all Eg changes, which occurred in response to various influences and defects, with the changes of the electron work function, which were experimentally measured by photoelectron emission (PE) technique. In this case for all the changes we can write $\Delta\varphi = \varphi - \varphi_0 = \mathrm{Eg} - \mathrm{Eg}_0 = \Delta\mathrm{Eg}$. So, calculated change ΔEg corresponds to measured changes of work function $\Delta\varphi$ corresponding to various defects and influences, obtained after any performed treatments.

Using our DOS calculations and corresponding experimental data, we analyzed the synchrotron excitation and following photoluminescence irradiation process and proposed the schematics, shown in Fig. 8. This process has several steps: 1) excitation by synchrotron irradiation in all ranges leads to transfer of excited electrons from valence band first from A, B, C, and D peaks and then from more deep levels, 2) relaxation of excited electrons to the bottom of the conductive band, 3) trapping of the relaxed electrons at the OH-vacancies energy levels Ei in the middle of the forbidden gap Eg, 4) recombination of the electron with holes at these energy levels, 5) irradiation of the luminescence photons with the average energy Ei $\sim$ 2.95 eV, intensity of which is comparable with the intensity of DOS peaks (A, B, C, and D) in the valence band from which electrons jumped (as schematically shown in Fig. 8 by marked arrows). The proposed process explains the obtained experimental data on synchrotron irradiation of the HAP samples after different performed treatments in accordance with observed changes in intensities and work function changes.

Computed data show that OH-vacancy shifts the forbidden gap from value Eg $\sim$ 4.6 eV for pure hexagonal HAP to the value of Eg $\sim$ 5.49 eV. The energy levels for OH-vacancy are Ei $\sim$ Ev + (3.0 – 3.8) eV from the top of the valence band or Ei $\sim$ Ec – (2.5 – 1.7) eV from the bottom of the conductive band. The energy levels for H inter-nodes are Ei $\sim$ Ev + (1.2 – 1.75) eV from the top of the valence band or Ei $\sim$ Ec – (3.9 – 3.4) eV from the bottom of the conductive band. Both type of the energy levels could serve for the recombination of electrons with holes and irradiation of PL photons with corresponding energy close to experimentally observed Ei $\sim$ 2.95 eV. It is worth noting that this peak at Ei $\sim$ 2.95 eV with half-width $\sim$1 eV (i.e., it varies in the range $\sim$2.4–3.4 eV) is experimentally observed average value of the sum from a lot of the various HAP unit cells, which could have different defects. Our modelled defects (OH vacancy and H inter-nodes) are only part of all possible situations. The computed energy obtained for both of these defects lies into the experimentally observed range. So, we can

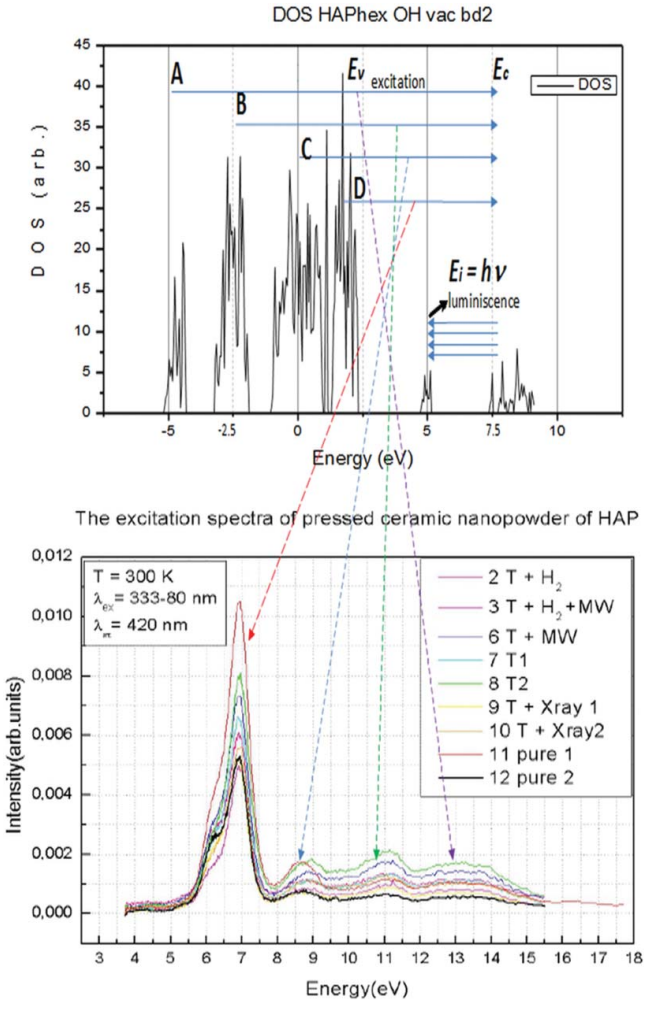

Figure 8. Schematics of the synchrotron excitation and photoluminescence processing through OH-vacancy energy levels as the traps for electron-holes recombination with irradiation of resultant photons with energy Ei $\sim$ 2.95 eV and equivalent wavelength $\lambda \sim$ 420 nm.

conclude that both defects could give their statistical contribution into formation of the total measured peak. But OH vacancies are preferable for this purpose, because the registered intensity of PL increases with rise of OH vacancies concentration after high temperature treatment, which is proportional to the annealing of OH vacancies at this high temperature.

5. Conclusion

The computational technique of the first principle calculations of HAP structures was developed using LDA DFT methods and applied for calculations in pure hexagonal and monoclinic HAP phases and in HAP structures with defects.

The calculations of defects were performed, e.g., hydrogen vacancy and inter-nodes, OH vacancy. Calculated DOS show the arising of the energy levels $E_{H\text{-}int} \sim Ei \sim Ev +$ (1.2 – 1.75) eV $\sim$ Ec – (3.9 – 3.4) eV for H inter-node, $E_{OH\text{-}vac} \sim Ei \sim Ev +$ (3.0 – 3.8) eV $\sim$ Ec – (2.5 – 1.7) eV for OH vacancy inside the forbidden gap Eg.

Computed data show that monoclinic phase with oppositely oriented OH ions in the neighboring channels has the lowest energy of ∼24 meV for "Ca2" model and of $\sim$ 2 meV for "Ca10" model in comparison with hexagonal HAP ordered phase.

The data obtained on HAP after temperature and microwave treatments show the increase of the PL emission peak at $\sim$ 2.95 eV (420 nm) and, then, series of the PL peaks (∼9 eV, 11 eV, 13 eV) at this PL line after synchrotron excitation in the interval 4–20 eV. These peaks are explained by the excitation from orbitals in valence band as follows from the developed model and DOS calculations. The intensity of these peaks increases after heating and microwave irradiation correspondingly to the increase of the OH vacancy defects. During following electron relaxation and trapping on the $E_{OH\text{-}vac}$ PL emission with ∼420 nm is observed.

Finally, all these data could be very useful for further development of technological control of the annealed OH vacancies and incorporated H during HAP treatment and other wide practical applications, which are necessary for HAP surface modification, such as its electrical charging.

Acknowledgments

This work is partially supported by the Riga Technical University (Latvia) and Ministry of Science and Education of Russian Federation.

Funding

VB acknowledges financial support via FCT Grant No. SFRH/BPD/22230/2005 (Portugal).

References

1. M. Epple, K. Ganesan, R. Heumann, J. Klesing, A. Kovtun, S. Neumann, and V. Sokolova, Application of calcium phosphate nanoparticles in biomedicine, J. Mater. Chem. **20** (1), 18–23 (2010).
2. B. Ratner, A. S. Hoffman, F. J. Schoen, and J. E. Lemons, eds.: Biomaterial Science. London: Academic Press; 1996 .
3. V. S. Bystrov, E. V. Paramonova, Yu Dekhtyar, A. Katashev, A. Karlov, N. Polyaka, A. V. Bystrova, A. Patmalnieks, and A. L. Kholkin, Computational and experimental studies of size and shape related physical properties of hydroxyapatite nanoparticles, J. Phys.: Condens. Matter. **23**, 065302 (2011).
4. V. S. Bystrov, N. K. Bystrova, E. V. Paramonova, and Yu. D. Dekhtyar, Interaction of charged hydroxyapatite and living cells: I. Hydroxyapatite polarization properties. Mathematical biology and bioinformatics. **4** (2), 7–11 (2009).
5. PERCERAMICS, Multifunctional percolated nanostructured ceramics fabricated from hydroxyapatite. - NMP3-CT-2003-504937 FP6 project. Final report Summary: (2008).
6. Yu Dekhtyar, N. Polyaka, and R. Sammons, Electrically charged hydroxyapatite enhances immobilization and proliferation of osteoblasts. IFMBE Proceedings, 14th Nordic-Baltic Conference on Biomedical Engineering and Medical Physics. **20**, 23–25 (2008).

7. Yu Dekhtyar, V. Bystrov, A. Bystrova, A. Dindune, A. Katashev, I. Khlusov, E. Palcevskis, E. Paramonova, N. N. Polyaka, M. Romanova, R. Sammons, and D. Veljović, Engineering of the hydroxyapatite cell adhesion capacity, IFMBE Proceedings. International Symposium on Biomedical Engineering and Medical Physics. **38**, 182–185 (2013).
8. M. A. Martins, C. Santos, M. M. Almeida, and M. E. V. Costa, Hydroxyapatite micro- and nanoparticles: Nucleation and growth mechanisms in the presence of citrate species, J. Coll. & Interface Sci. 210–216 (2008).
9. V. Bystrov, E. Costa, S. Santos, M. Almeida, A. Kholkin, S. Kopyl, Yu Dekhtyar, A. V. Bystrova, and E. V. Paramonova, Computational study of hydroxyapatite properties and surface interactions, IEEE Conf. Publications. 1–3 (2012).
10. N. Y. Mostafa, and P. W. Brown, Computer simulation of stoichiometric hydroxyapatite: structure and substitutions, J. Phys. Chem. Solids. **68**, 431 (2007).
11. S. A. M. Tofail, D. Harvety, K. T. Stanton, and J. B. McMonagle, Structural order and dielectric behavior of hydroxyapatite, Ferroelectrics. **319** (1), 117–123 (2005).
12. A. Slepko, and A. A. Demkov, First-principles study of the biomineral hydroxyapatite, Phys. Rev. B. **84**, 134108 (2011).
13. K. Matsunaga, and A. Kuwabara, First-principles study of vacancy formation in hydroxyapatite. Phys. Rev. B. **75**, 014102 (2007).
14. V. S. Bystrov, E. V. Paramonova, M. E. Costa, C. Santos, M. Almeida, S. Kopyl, Yu Dekhtyar, A. V. Bystrova, E. I. Maevsky, R. C. Pullar, and A. L. Kholkin, Computational study of hydroxyapatite properties and surface interactions. Ferroelectrics. **449**, 92–101 (2013).
15. D. Aronov, M. Chaikina, J. Haddad, A. Karlov, G. Mezinskis, L. Oster, I. Pavlovska, and G. Rosenman, Electronic states spectroscopy of hydroxyapatite ceramics, J. Mater. Sci.: Mater. Med. **18** (5) 865–870 (2007).
16. A. V. Bystrova, Yu Dekhtyar, A. I. Popov, and V. S. Bystrov, Modeling and synchrotron data analysis of modified hydroxyapatite structure. Mathematical Biology and Bioinformatics. **9** (1) 171–182 (2014).
17. V. S. Bystrov, J. Coutinho, A. V. Bystrova, A. I. Popov, and Yu Dekhtyar, Computational study of the hydroxyapatite structures, properties and defects, J. Phys. D: Appl. Phys. in print (2014).
18. http://aimpro.ncl.ac.uk/
19. HyperChem, Tools for molecular modeling (release 7, 8). Gainnesville: Hypercube, Inc.: 2002.
20. V. Pankratov, A. I. Popov, A. Kotlov, and C. Feldman, Luminescence of nano- and macrosized $LaPO_4$:Ce, Tb excited by synchrotron radiation. Optical Materials. **33**, 1102–1105 (2011).